Hardness identification of rock based on multi-sensor information fusion during the process of roadway tunnelling

H. WANG[1], S. LU[1], M. HUANG[1], and X. ZHAO[2*]

[1] Guangxi Key Laboratory of Manufacturing System and Advanced Manufacturing Technology, School of Mechanical
and Electrical Engineering, Guilin University of Electronic Technology, Guilin Guangxi, China
[2] School of Electronic Engineering and Automation, Guilin University of Electronic Technology, Guilin, Guangxi, China

Abstract. In this paper, a new dynamic model was proposed for identifying the rock hardness during the process of roadway tunnelling, thereby regulating the speed of the driving motor and the torque of the cutting head. The presented identification model establishes a multi-information feature database containing vibration signals in the y-axis, acoustic emission signals, cutting current signals, and temperature signals. Subsequently, we obtain the membership functions (MFs) of the given multiple signals with the amount of feature samples according to the principle of minimum fuzzy entropy. Furthermore, a rock hardness identification model was established based on multi-sensor information fusion and Dempster-Shafer (D-S) evidence theory. To prove the accuracy of the proposed model, an identification experiment was carried out through the cutting of a poured mixed rock specimen with five grades of hardness. As a result, the proposed identification model recognizes the rock hardness accurately for fifteen sampling points, which indicates the significance of the method with regard to the dynamic identification of rock hardness during the process of roadway tunnelling, and further provides data support for adjusting the speed of the cutting head adaptively, thereby achieving high efficiency tunnelling.

Key words: Rock hardness identification, membership function, information fusion, Dempster-Shafer.

1. Introduction

Road headers applied to urban traffic and mine roadways, railways, and highways are widely used to tunnel straight underground roadways. A road header mainly contains of four separate mechanisms for walking, working, shipping, and trans-shipping [1]. During the process of tunnelling, the road header cuts rock through the reciprocating oscillation of a cutting head [2]. Thus, the tunnelling rate has a significant relation with the hardness of rock. Many previous researches have shown that an increasing tunnelling rate always accompanies a decrease in rock hardness under different rock properties [3]. Rock characteristics and geological environment of a long-distance tunnelling face are influenced by a variety of factors, and therefore the hardness of rock in different driving positions is significantly different. A traditional tunnelling method with a constant feed speed is unable to be adaptively regulated for different degrees of rock hardness. For example, the tooth of a cutting head will be seriously worn or even broken when the rock is too hard, as shown in Fig. 1. Thus, the speed of the cutting head while tunnelling should be reduced under a high hardness condition, and in contrast, the speed should be increased along with a decrease in hardness to improve the working efficiency of the road header, thereby accelerating the construction progress. All previous analyses have indicated that

(a)   (b)

Fig. 1. Worn and broken tooth of the cutting head: a) Worn tooth;
b) Broken tooth

a method for monitoring the hardness of rock online during the tunnelling process is an urgent issue.

Several related researches have been presented to solve the above issues. Yang et al. presented a hardness identification model for both coal and rock based on the frequency-domain energy characteristics of vibration signals [4]. They extracted the frequency-domain indexes under different cutting conditions, indirectly determining the hardness of the cutting medium. In addition, they utilised the weighted averages method to solve the fuzzy membership functions (MFs) of the cutting hardness, and combined with the defined cutting hardness factor, the coal and rock properties were finally identified [5]. Utt used measurements taken while a layer is being drilled, one can convert the data to suitably scaled features and classify the strength of the layer with a neural network [6]. Improvement made by Kahraman and Rostami in characterization of rock and rock mass fea-

tures allowed the improved understanding of ground conditions and rock mass classifications [7]. Using MATLAB, Li et al. established a load mathematical model for the cutting head, and further analysed the load of a road header under different rock hardness conditions. The load characteristics and a change in the rules of power were obtained [8]. Szwedzicki used an indentation testing method for characterisation of the hardness of rock materials, which reflects a relationship between the values of the indentation hardness index and the uniaxial compressive strength, and thus the value of the calculated index can be used to classify the hardness of rock [9]. Yaar et al. focused on the statistical relations between physico-mechanical properties and rock hardness, and further found that such properties can be estimated using hardness methods, as well as through a comparison with the calculated values from different empirical equations [10]. Shalabi et al. studied different types of rocks encountered in engineering projects and found that there are good relationships between the engineering properties of intact rock and its hardness [11]. With normalised MWD data, van Eldert found it was possible to mimic the tunnel contour mapping, and the results showed good correlation with mapped Q-value and installed rock support. MWD technology can improve the accuracy of forecasting the rock mass ahead of the face [12].

However, the abovementioned previous studies placed particular emphasis on theoretical research and recognition with a single signal, and thus the recognition accuracy is relatively low. Therefore, a new method for identifying the hardness of rock is urgent to improve the accuracy of coal-rock recognition, and thereby adjust the speed of the cutting head in an adaptive manner.

This paper presented a new method to identify hardness of rock accurately by multiple information fusion. The remainder of this paper is organized as follows. First, we tested the feature signals used for fusion during the process of roadway tunnelling. Next, five kinds of rock specimens with different hardness were poured, and five group cutting experiments were carried out on poured specimens to obtain the databases of each feature signal. Moreover, according to the rule of minimum fuzzy entropy, the membership functions of each feature signal were optimized. Combined with an AND decision rule, a multi-information fusion model was established to identify the hardness of rock. Finally, the accuracy of the proposed rock hardness identification model based on multi-information fusion are provided through experiments.

2. Feature signal testing and analysis

2.1. Multi-feature signal analysis of tunnelling.
During the process of tunnelling, the tangential force, radial force, and lateral force have significantly different tooth owing to their different installation angles. Furthermore, the tangential force, radial force, and lateral force can be separately decomposed into the three axes, namely, f_{x_i}, f_{y_i}, and f_{z_i} [13], as shown in Fig. 2, n represent the number of teeth installed in a cutting head. In addition, F_x, F_y, and F_z indicate the resultant forces in the axes of x, y, and z, respectively.
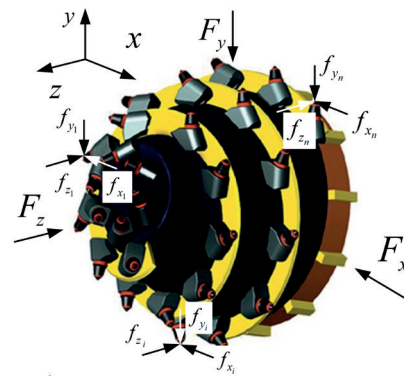

Fig. 2. Force analysis of a cutting head

The cutting vibrations are consistent with the direction of the beard 3D force, which contains a transverse vibration along the x-axis, a longitudinal vibration along the y-axis, and an axial vibration along the z-axis. We obtained tri-axial vibration acceleration curves of the cutting head while cutting hard rock by installing a tri-axial vibration acceleration sensor on a swivel lug. As shown in Fig. 3, clear vibrations were generated in
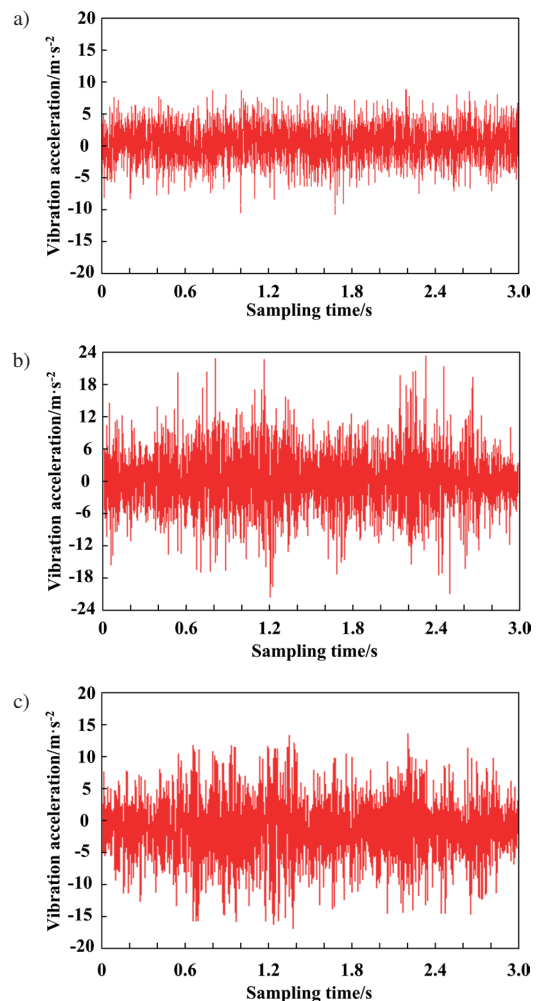

Fig. 3. Tri-axial vibration acceleration signals: a) x-axis; b) y-axis; c) z-axis

along x-, y-, and z-axes. The maximum absolute values of the vibration accelerations in the x-, y-, and z-axes are 11.35, 23.62, and 17.24 m·s^{-2}, respectively. Furthermore, lots of tests validate that the amplitude degree of vibrations in the process of cutting hard rock is in order of the y-, z-, and x-axes. Considering that plethoric signals will lead to larger dimensions of the recognition system, thereby reducing the response speed of the system, the vibration in the y-axis was applied as a feature signal of the presented identification system.

During the course of tunnelling hard rock, the cutting currents change dramatically along with the change in cutting resistance owing to the varying hardness of the rock, as shown in Fig. 4. In addition, sharp collisions and friction occur between the picks and hard rock while tunnelling, which generates both a significant acoustic emission phenomenon and an instantaneous flash temperature zone on the surface of the pick, namely, the flash temperature [14], as shown in Figs. 5 and 6, separately. Thus, tests regarding the changes in cutting current, acoustic emissions, and flash temperature while tunnelling rock with different degrees of hardness are capable of reflecting the changes in rock hardness.
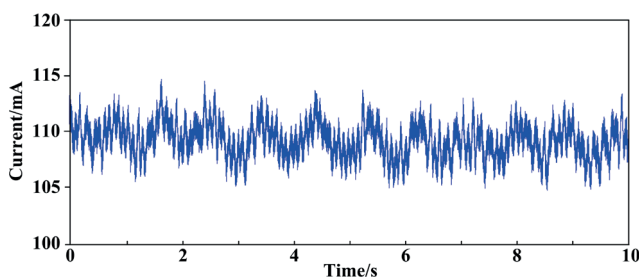
Fig. 4. Tunnelling current
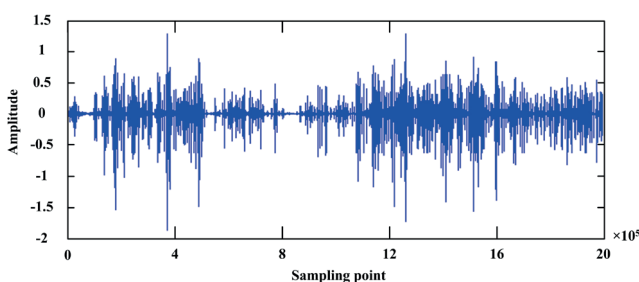
Fig. 5. Acoustic emission signal while tunnelling
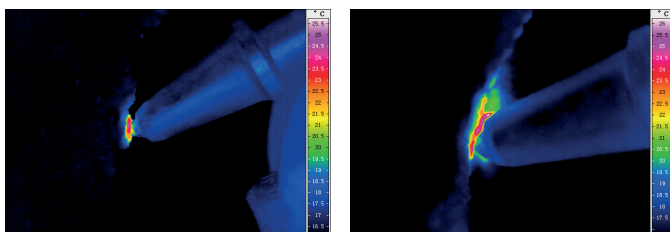
Fig. 6. Instantaneous flash temperature while tunnelling

2.2. Extraction and recognition of multi-feature signals.
The hardness of rock can be divided into five grades, as listed in Table 1. The hardness of rock is generally represented through a

Table 1
Hardness of rock of different grades

Hardness grade	Representative rock	Protodyakonov coefficient
G_1	argillaceous rock	4
G_2	sandstone	6
G_3	conglomerate	10
G_4	granite	15
G_5	quartzite, basalt	20

Protodyakonov coefficient. The Protodyakonov coefficient represents the relative value of rock resistance to crushing. As the rock has the strongest compressive strength, ten percent of uniaxial compressive strength limit is defined as the Protodyakonov coefficient, which is expressed as

$$f = R/100, \qquad (1)$$

where f is the hardness of rock, R is the one-way uniaxial ultimate compressive strength of a standard sample of rock in kg·cm^{-2}.

A test-bed was established for testing the multi-feature signals, as shown in Fig. 7. The test-bed of a road header should comprehensively consider the mechanical structure of road header, cutting theory, similarity theory and similarity coefficient. However, this paper is devoted to recognizing the rock hardness effectively according to the differences of multi-feature signals in the cutting process. Thus, the test-bed should realize the similar functions of walking and cutting, capable to obtain the signals with similar regularity. The vibration signals were tested using a vibration sensor. A thermal infrared imager was used to collect the flash temperature signal, and we obtained the current signal of the cutting motor through an electrical parameter acquisition module. In addition, the acoustic emission signals were tested and extracted using an acoustic emission sensor and its acquisition system.
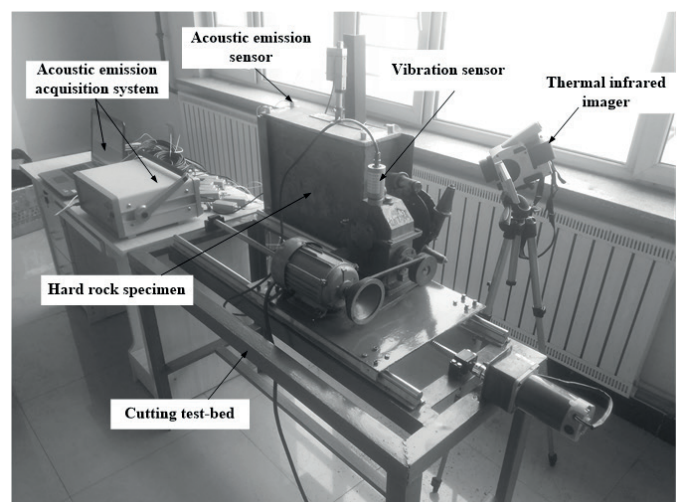

Fig. 7. Test-bed for hard rock cutting

The rock specimens with different hardness grades have corresponding proportion of sand and cement. The proportion of sand and cement with different hardness grades is determined through a large number of experiments and tests. Then, five kinds of rock specimens with different hardness were poured in a laboratory, and we tested the Protodyakonov coefficient of each, as listed in Table 2.

Table 2
Protodyakonov coefficients of rock specimens

Hardness grade	G_1	G_2	G_3	G_4	G_5
Protodyakonov coefficient	3.8	6.4	10.3	14.6	18.8

Several cutting experiments were carried out to test the multiple signals of hard rock with five given tested Protodyakonov coefficients. The features of each signal were extracted as follows:
1. Signals of vibration and acoustic emission. Both vibration signals and acoustic emission signals were decomposed and reconstructed through a wavelet packet analysis. The energy levels of the vibration signals and acoustic emission signals, which change regularly with the change in hardness, were extracted as feature samples.
2. Flash temperature signals. During the process of cutting, infrared thermal images were taken using a thermal infrared imager, and the flash temperature feature was obtained using IRBIS3 Plus analysis software.
3. Cutting current signals. An electricity parameter acquisition module was used to test the cutting current signals and then the root mean square (RMS) values were obtained by analysing the tested current signals.

The samples of each feature signal while cutting the given rock specimens were organized, as shown in Tables 3 and 6.

Table 4
Sample values of acoustic emission signals

Serial number	Acoustic emission energy				
	G_1	G_2	G_3	G_4	G_5
1	50.8	57.6	64.8	72.3	82.9
2	51.6	58.1	65.4	72.9	83.7
3	52.1	58.6	66.2	73.8	84.6
4	52.9	59.3	66.8	74.6	85.8
5	53.7	59.9	67.5	75.7	87.1
6	54.3	60.6	68.4	76.4	89.0
7	54.8	61.4	69.2	77.8	90.5
8	55.6	62.1	69.8	78.6	91.3
9	56.1	62.9	70.5	79.4	92.7
10	56.7	63.6	71.2	80.7	93.5
11	57.4	64.1	71.8	81.5	95.4
12	58.0	65.2	72.6	82.3	96.5
13	58.5	65.9	73.4	83.1	97.4
14	58.9	66.7	73.9	84.2	98.3
15	59.6	67.6	74.6	84.9	99.7

Table 3
Sample values of vibration signals

Serial number	Vibration energy				
	G_1	G_2	G_3	G_4	G_5
1	105.8	118.6	131.6	144.5	162.8
2	106.3	119.2	132.5	145.9	164.2
3	107.9	120.3	133.4	147.6	165.8
4	109.2	121.5	134.6	149.2	167.5
5	110.5	122.0	135.8	150.8	169.4
6	112.3	123.1	137.2	152.9	171.6
7	113.4	125.3	138.9	154.3	173.2
8	114.7	126.7	140.1	155.8	175.8
9	116.2	128.2	142.3	157.5	178.5
10	117.5	129.6	143.8	159.2	180.6
11	118.8	130.5	144.9	161.0	183.1
12	119.6	131.4	146.2	162.7	185.9
13	121.1	132.6	147.5	164.3	187.4
14	122.3	133.9	148.9	166.2	189.2
15	122.9	134.4	149.4	167.2	191.5

Table 5
Sample values of temperature signals

Serial number	Temperature (°C)				
	G_1	G_2	G_3	G_4	G_5
1	25.6	29.5	33.9	39.2	44.9
2	25.9	29.8	34.3	39.6	45.6
3	26.1	30.2	34.6	40.1	46.7
4	26.4	30.7	35.1	40.8	47.2
5	26.8	31.1	35.8	41.5	47.8
6	27.1	31.6	36.4	41.9	48.5
7	27.6	32.0	36.9	42.6	49.3
8	27.9	32.4	37.3	43.1	49.9
9	28.1	32.7	37.7	43.5	50.6
10	28.5	33.1	38.2	44.2	51.1
11	29.0	33.5	38.8	44.7	51.9
12	29.4	33.7	39.2	45.3	52.8
13	29.6	34.2	39.9	45.8	53.9
14	30.1	34.8	40.3	46.5	55.4
15	30.4	35.2	40.7	47.2	56.1

Table 6
Sample values of current signals

Serial number	Current (A)				
	G_1	G_2	G_3	G_4	G_5
1	1.026	1.151	1.302	1.428	1.590
2	1.038	1.170	1.313	1.435	1.604
3	1.054	1.183	1.626	1.449	1.617
4	1.067	1.196	1.341	1.461	1.628
5	1.088	1.205	1.352	1.475	1.644
6	1.095	1.218	1.359	1.489	1.656
7	1.109	1.229	1.371	1.503	1.667
8	1.117	1.243	1.388	1.517	1.682
9	1.126	1.258	1.395	1.529	1.688
10	1.139	1.274	1.407	1.544	1.695
11	1.148	1.289	1.419	1.567	1.699
12	1.156	1.306	1.436	1.579	1.702
13	1.172	1.317	1.448	1.593	1.706
14	1.194	1.326	1.462	1.611	1.711
15	1.203	1.340	1.476	1.623	1.713

3. Multi-information fusion model

3.1. Optimal combination algorithm of Dempster-Shafer.
An identification framework Θ of the rock hardness consists of five proposed hardness grades of G_1 to G_5, and is expressed as $\{Q_1, Q_2, Q_3, Q_4, Q_5\}$ [15, 16]. The basic probability assignments of each feature signal are represented as m_1, m_2, m_3, m_4 and m_5, respectively. In addition, set Bel_1 and Bel_2 to be the belief functions in identification framework 2^Θ, and their basic probability assignments and kernels are respectively expressed as m_1 and m_2, $\{A_1, A_2, \ldots, A_q\}$ and $\{B_1, B_2, \ldots, B_q\}$. If $\sum_{i=j, A_i \cap B_j = \emptyset} m_1(A_i) m_2(B_j) < 1$, while the fusion was finished based on D-S, the equation of basic probability assignment is expressed as

$$m(A) = \begin{cases} 0 & A = \emptyset \\ (1-k)^{-1} \sum_{A_i \cap B_j = A} m_1(A_i) m_2(B_j) & A \neq \emptyset \end{cases} \quad (2)$$

where $m(A)$ is the basic probability assignment, k reflects the levels of conflict among varying evidence, $k = \sum_{A_i \cap B_j = \emptyset} m_1(A_i) m_2(B_j)$.

According to Eq. (2), the evidence combination rule of multiple belief functions is deduced as

$$m = (((m_1 \oplus m_2) \oplus m_3) \oplus \cdots) \oplus m_n, \quad (3)$$

where $m_1, m_2, \ldots, m_n$ represent the basic probability assignments of belief functions $Bel_1, Bel_2, \ldots, Bel_n$ in the same identification framework, 2^θ, respectively.

During the process of multiple information fusion, the evidence of various types of information may conflict with each other owing to the diversity and uncertainty of the feature samples. In general, the greater the degree of evidence supported by other types of evidence, the more credible the evidence will be otherwise, a lower credibility is considered. If the credibility $Crd(m_i)$ of the evidence is regarded as a weight, the condition $\sum_{i=1}^{q} Crd(m_i) = 1$ should be satisfied. Thus, conflicting data can be processed based on the weight of all evidence obtained. The D-S combination rules are then used for identification and fusion, thereby modifying and optimizing the traditional Dempster-Shafer model.

Given $\beta_i = Crd(m_i)$, $i = 1, 2, \ldots, q$, the pre-treatment of the conflicting evidence m_i, $(i = 1, 2, \ldots, q)$ is expressed as

$$m'_i = \beta_i m_i, \qquad i = 1, 2, \ldots, q. \quad (4)$$

The optimized combination rules are then revised as follows:

$$\begin{cases} m(A) = \dfrac{1}{1-k'} \sum_{A_i \cap A_j = A} m'_1(A_i) m'_2(A_j), & A \neq \emptyset \\ m(\emptyset) = 0 \end{cases} \quad (5)$$

where $k' = \sum_{A_i \cap A_j = \emptyset} m_1(A_i) m_2(A_j)$.

3.2. Membership function optimization model.
A multi-information fusion model for hardness identification of rock was established based on the probability distribution function. However, the probability distribution function is merely an inference for the reliability of the targets. Thus, the probability distribution formula of a reliability function was constructed based on the MFs [17]. There are several categories of MFs, but trapezium and triangular MFs among them are most widely used owing to their simplicity and convenience. Thus, in this paper, trapezium and triangular MFs are used to establish an MFs model of each cutting feature signals for identifying the hardness of rock, which is shown in Fig. 8.
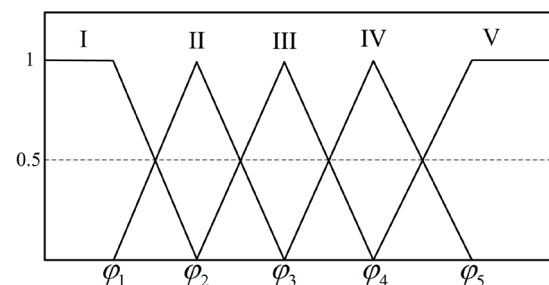

Fig. 8. MF model of hardness identification

A fuzzy entropy is capable to describe the fuzziness degree of a fuzzy set. If a fuzziness of a fuzzy set is small, its fuzzy entropy must be very small. Otherwise, a large fuzziness of a fuzzy set always leads to a large fuzzy entropy [18]. Specifically, the fuzzy entropy of a definite set is zero, namely, without

fuzziness. Conversely, [1/2] has a maximum fuzzy entropy, and the fuzzy entropy decreases from [1/2] to the definite set [19].

Let $\mu(x)$ be a MF of a fuzzy set X, which is expressed as $X = \{x_1, x_2, \ldots, x_n\}$. The fuzzy entropy of X is shown as below

$$S(Q_j) = \begin{cases} 0 & \alpha = 0 \\ -\dfrac{1}{n \ln 2} \sum\limits_{i=1}^{n} [\alpha \ln \alpha + (1-\alpha) \ln(1-\alpha)] & \alpha \subset (0,1) , \\ 0 & \alpha = 1 \end{cases} \tag{6}$$

where $\alpha = \mu_j(x_i)$.

An ideal MF is capable to reflect the fuzziness of a fuzzy set as well as the actual hardness of rock by the obtained evidence, accurately. Therefore, ensuring that the MF can correctly reflect the fuzziness, and then minimized the value of fuzzy entropy to effectively reflect the true rock tunnelling conditions [20]. According to the established MFs shown in Fig. 5, calculating the thresholds φ_i by Eq. (7) based on the minimum fuzzy degree [21].

$$S_{\min}(Q_1, Q_2, \ldots, Q_5) = -\frac{1}{n \ln 2} \sum_{i=1}^{n} \sum_{j=1}^{5} \left\{ \mu_j(x_i) \ln \mu_j(x_i) \right. \tag{7}$$
$$\left. + (1 - \mu_j(x_i)) \ln(1 - \mu_j(x_i)) \right\},$$

where n is the sample size of the fuzzy set, and x_i denotes the i-th sample.

According to the obtained samples of each feature signal shown in Tables 3 to 6, the thresholds corresponding to different signals are used as independent variables, and then solve the minimum value of the equation based on principle of minimum fuzzy entropy. Meanwhile, the optimized thresholds corresponding to each signal are obtained.

When $j = 1$ or $j = 5$, a trapezium MF is used, and the formula of $\mu(x)$ is

$$\mu_1(x) = \begin{cases} 1 & (x \le \varphi_1) \\ \dfrac{\varphi_2 - x}{\varphi_2 - \varphi_1} & (\varphi_1 < x < \varphi_2) ; \\ 0 & (\text{else}) \end{cases}$$

$$\mu_5(x) = \begin{cases} 1 & (\varphi_5 \le x) \\ \dfrac{\varphi_5 - x}{\varphi_5 - \varphi_4} & (\varphi_4 < x < \varphi_5) . \\ 0 & (\text{else}) \end{cases}$$

Otherwise, when $j = 2$, 3, or 4, a triangular MF is used, and the formula of $\mu(x)$ is

$$\mu_j(x) = \begin{cases} \dfrac{x - \varphi_{j-1}}{\varphi_j - \varphi_{j-1}} & (\varphi_{j-1} < x < \varphi_j) \\ \dfrac{\varphi_{j+1} - x}{\varphi_{j+1} - \varphi_j} & (\varphi_j < x < \varphi_{j+1}) . \\ 0 & (\text{else}) \end{cases}$$

The feature samples in Tables 3 and 4 possess definite fuzziness [22]. Thus, according to Eq. (7), a solver based on MATLAB was adopted to calculate the values of thresholds φ_i and optimize the MFs. Then, each optimized membership function of each feature signal was obtained, as shown in Fig. 9.
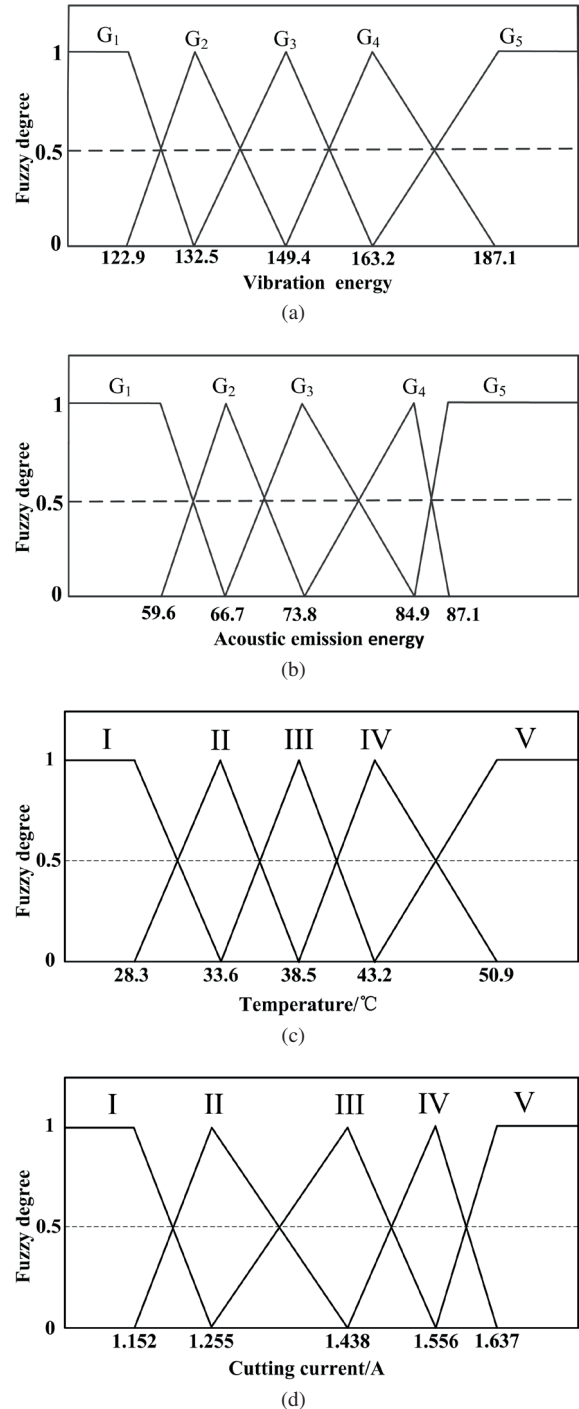

Fig. 9. The optimized MFs: a) Vibration signal; b) Acoustic emission signal; c) Temperature signal; d) Current signal

3.3. Basic probability assignments functions.
According to the given definition, m_1, m_2, m_3, and m_4 represent the basic probability assignments of each feature signal, respectively.

Thus, the formulas of the basic probability assignment functions $m_i(Q_j)$ of each fuzzy subset, and the non-determinacy $m_i(\Theta)$ given to the evidence bodies, are expressed as

$$m_i(Q_j) = \frac{\mu_i(Q_j)}{\sum_j \mu_i(Q_j) + 1 - \kappa_i \cdot \vartheta_i \cdot \delta_i}, \quad (8)$$

$$m_i(\Theta) = \frac{1 - \kappa_i \cdot \vartheta_i \cdot \delta_i}{\sum_j \mu_i(Q_j) + 1 - \kappa_i \cdot \vartheta_i \cdot \delta_i}, \quad (9)$$

where κ_i is the difference value between the maximum and second largest membership degrees of the i-th evidence, as shown in Formula (10), which is capable to express the reliability of the identification. ϑ_i, expressed in Formula (11), is the variance of membership degree that the i-th evidence belongs to the rest rock hardness except the maximum membership degree. which reflects the reliability of the decision, and δ_i denotes the weight of the i-th evidence. In addition, $1 - \kappa_i \cdot \vartheta_i \cdot \delta_i$ denotes the total uncertainty during the identification process.

$$\kappa_i = \mu_i(Q_m) - \max_{j \neq m} \{\mu_i(Q_j)\}, \quad (10)$$

$$\vartheta_i = \sqrt{\frac{1}{N-1} \sum_{j=1}^{M} (\mu_i(Q_j) - \xi_i)^2}, \quad (11)$$

where $\mu_i(Q_m)$ denotes the maximum value of the fuzzy degree, in which the i-th evidence belongs to the m-th proposition, which is expressed as $\max_j \{\mu_i(Q_j)\}$. In addition, ξ_i denotes the mean value of the fuzzy degree with the exception of the maximum, which is expressed as $\frac{1}{M-1} \sum_{j=0, j \neq m}^{M} \mu_i(Q_j)$.

3.4. Basic decision rules of information fusion. To recognize the hardness of rock accurately while tunnelling, the recognition results of rock's hardness should possess the maximal reliability [23–25], as well as reducing the non-determinacy of the recognition results to minimum. Thus, an AND decision method, contains multiple rules, was proposed to ensure the effectiveness of decision results. The AND decision method consist of three rules:

Rule 1: $Bel(A_m) = \max_j \{m(A_j)\}$,

Rule 2: $Bel(A_m) - Bel(A_j) > \tau 1$,
$Bel(A_m) - m_i(\theta) > \tau \ (\tau > 0 \text{ and } \tau \in R)$,

Rule 3: $m_i(\theta) < \lambda \ (\lambda > 0 \text{ and } \lambda \in R)$.

Rule 1 requires the hardness identification results of rock possess the maximal reliability. Rule 2 ensures that the difference value of reliability between the recognition result and other propositions be greater than the threshold τ. According to rule 3, the uncertainty of the identification result is limited with λ. The thresholds τ and λ are mainly determined by experience or number of experiments. An effective recognition result of hardness must satisfy three rules of AND decision simultaneously. Once one among three decision rules is not satisfied, it indicates that the recognition system has no correct result, namely, the hardness recognition results of rock cannot be obtained.

4. Experiments

A mixed rock specimen consisting of five hardness grades was poured to verify the recognition accuracy and reliability of the hardness identification model for rock, as shown in Fig. 10. Fifteen sampling points were estimated in total and were equally distributed among rocks with different hardness levels. Cutting experiments were then carried out to test the multiple signals and extract the feature data on the vibration, current, temperature, and acoustic emissions, as shown in Table 7. Finally, the hardness of the rock samples was identified using the multi-information fusion model based on the D-S theory and AND decision method. According to the previous experimental results and experience, the threshold value of τ and λ should be
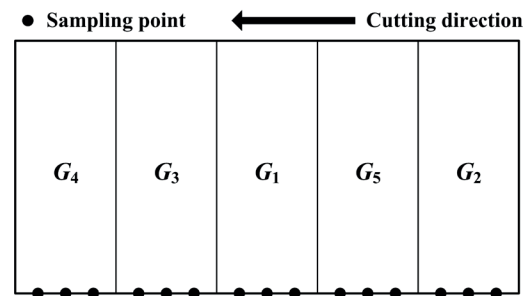

Fig. 10. Mixed rock specimen and sampling points

Table 7
The feature signals of 15 sampling points

Sampling point	Vibration energy	Acoustic emission	Temperature/°C	Current/A
1	130.6914	64.2952	31.92	1.4941
2	130.4216	63.5213	31.17	1.3114
3	130.1662	64.4443	31.97	1.4903
4	182.3487	86.5384	48.191	1.5045
5	183.8138	86.5749	48.31	1.4985
6	185.6588	79.4488	48.88	1.3483
7	124.3064	60.8397	30.28	1.3324
8	124.3064	60.6977	30.39	1.3324
9	123.7467	70.2102	25.56	1.4916
10	150.3770	63.4965	37.06	1.5895
11	136.6077	77.5363	35.99	1.5909
12	150.3494	64.0581	36.79	1.5946
13	157.8939	85.4157	41.19	1.3593
14	169.1415	85.4672	46.06	1.4987
15	168.6635	85.4232	46.10	1.5051

H. Wang, S. Lu, M. Huang, and X. Zhao

Table 8
Identification results of hardness based on three information fusions without temperature

Actual hardness grade	$m_j(Q_1)$	$m_j(Q_2)$	$m_j(Q_3)$	$m_j(Q_4)$	$m_j(Q_5)$	$m_j(\theta)$	Identification result
G_2	0.1412	**0.7377**	0.0421	0.0373	0	0.0417	G_2
G_2	0.0942	**0.8505**	0.0283	0	0	0.0270	G_2
G_2	0.1668	**0.6781**	0.0583	0.0465	0	0.0502	G_2
G_5	0	0	0.0225	0.2269	**0.7265**	0.0241	—
G_5	0	0	0.0176	0.1656	**0.7971**	0.0196	G_5
G_5	0	0.0293	0.0870	0.1206	**0.7302**	0.0327	G_5
G_1	**0.8173**	0.1542	0.0138	0	0	0.0147	G_1
G_1	**0.8371**	0.1378	0.0122	0	0	0.0129	G_1
G_1	**0.6272**	0.1563	0.1316	0.0405	0	0.0442	—
G_3	0.0379	0.0461	**0.6221**	0.2138	0.0391	0.0411	—
G_3	0	0	**0.7064**	0.2430	0.0244	0.0261	—
G_3	0.0358	0.0604	**0.6961**	0.1384	0.0329	0.0364	G_3
G_4	0	0.0280	0.0371	**0.7952**	0.1098	0.0299	G_4
G_4	0	0	0.0224	**0.8663**	0.0863	0.0250	G_4
G_4	0	0	0.0171	**0.8994**	0.0652	0.0183	G_4

Table 9
Identification results of hardness based on four information fusions

Actual hardness grade	$m_j(Q_1)$	$m_j(Q_2)$	$m_j(Q_3)$	$m_j(Q_4)$	$m_j(Q_5)$	$m_j(\theta)$	Identification result
G_2	0.1127	**0.8460**	0.0143	0.0127	0	0.0142	G_2
G_2	0.0994	**0.8737**	0.0137	0	0	0.0131	G_2
G_2	0.1339	**0.8134**	0.0198	0.0158	0	0.0170	G_2
G_5	0	0	0.0085	0.1816	**0.8008**	0.0091	G_5
G_5	0	0	0.0062	0.1253	**0.8615**	0.0070	G_5
G_5	0	0.0083	0.0247	0.0821	**0.8756**	0.0093	G_5
G_1	**0.8623**	0.1264	0.0055	0	0	0.0058	G_1
G_1	**0.8716**	0.1179	0.0051	0	0	0.0054	G_1
G_1	**0.8368**	0.1043	0.0358	0.0110	0	0.0120	G_1
G_3	0.0136	0.0498	**0.8307**	0.0768	0.0140	0.0147	G_3
G_3	0	0.0146	**0.8107**	0.1446	0.0145	0.0155	G_3
G_3	0.0145	0.0638	**0.8378**	0.0559	0.0132	0.0147	G_3
G_4	0	0.0133	0.0476	**0.8726**	0.0522	0.0142	G_4
G_4	0	0	0.0087	**0.9061**	0.0756	0.0096	G_4
G_4	0	0	0.0067	**0.9290**	0.0572	0.0071	G_4

set to 0.5 and 0.05 to obtain the highest accuracy of recognition. The identified grades of hardness are listed in Tables 8 and 9.

Table 8 shows the identification results of hardness based on three information fusions without temperature. Obviously, four groups cannot obtain the right identification result according to the settled threshold value of τ and λ. As shown in Table 9, the identification results of the settled sampling points are consis-

tent with the actual hardness of rock. The minimum value of reliability that represents the recognition result is 0.8008, which is larger than that of other propositions, and the difference value of reliability between the recognition result and other propositions be greater than 0.5. Moreover, the uncertainty of each identification result is smaller than 0.05. Thus, the proposed hardness identification model of rock has a high identification accuracy and a good reliability.

Hardness identification of rock based on multi-sensor information fusion during the process of roadway tunnelling

5. Conclusions

According to the hardness identification results of rock by experiment, the proposed identification model has been proved to possess several advantages, which can be summarized as follows:

- Multiple signals, consisting of vibration, acoustic emissions, temperature, and current, were tested and extracted to obtain the feature samples of the information fusion model.
- According to the obtained feature sample database of multiple signals, the MFs were optimized based on the minimum fuzzy entropy.
- A basic probability assignment and decision rules were established to modify and optimize the traditional D-S model, and an optimization algorithm, which contains a combination of conflicting evidence, was used to improve the accuracy of identification.
- The fifteen identification results are consistent with the actual hardness of rock, which proves that the identification model has higher recognition accuracy and reliability.

References

[1] H.M. Mao, K. Chen, and H.H. Feng, "Rock-breaking mechanism of TBM with different types of cutter tools and estimation of thrust force", *Chinese J. Geo-tech. Eng.* 35 (9), 1627–1633 (2013).

[2] L.J. Zhao, X.N. Liu, and T. Cao, "Horizontal swing movement parameters optimization design of longitudinal road header", *J. China Coal Soc.* 37 (12), 2112–2117 (2012).

[3] K.Z. Song, H.X. Yang, K. An, *et al.*, "Shield tunnelling rate prediction model for complex rock stratum", *J. Highw. Transp. Res. Dev.* 25 (11), 105–108 (2008).

[4] J.J. Yang, H. Jiang, X.D. Ji, *et al.*, "Vibration identification method of coal and rock hardness based on wavelet packet features", *Coal Sci. Technol.* 43 (12), 114–117, 179 (2015).

[5] J.J. Yang, S.C. Fu, H. Jiang, *et al.*, "Recognition of cutting hardness of coal rock properties based on fuzzy criteria", *J. China Coal Soc.* 40 (S2), 540–545 (2015).

[6] W.K. Utt., "Neural network technology for strata strength characterization", in *Proceedings of the International Joint Conference on Neural Networks* 6 (1), 3806–3809 (1999).

[7] S. Kahraman, J. Rostami, and A. Naeimipour, "Review of ground characterization by using instrumented drills for underground mining and construction", *Rock Mech. Rock Eng.* 49 (2), 585–602 (2016).

[8] X.H. Li and L.L. Jiang, "Excavator loading simulation for hard-rock cutting", *Chinese J. Constr. Mach.* 6 (4), 415–417, (2008).

[9] T. Szwedzicki, "Indentation hardness testing of rock", *Int. J. Rock Mech. Min. Sci.* 35 (6), 825–829 (1998).

[10] E. Yaşar and Y. Erdoğan, "Estimation of rock physicomechanical properties using hardness methods", *Eng. Geol.* 71 (34), 281–288 (2004).

[11] F.I. Shalabi, E.J. Cording, and O.H. Al-Hattamleh, "Estimation of rock engineering properties using hardness tests", *Eng. Geol.* 90 (34), 138–147 (2007).

[12] J. van Eldert, H. Schunnesson, D. Johansson, *et al.*, "Application of Measurement while drilling technology to predict rock mass quality and rock support for tunnelling", textit*Rock Mech. Rock Eng.* 53 (3), 1349–1358 (2020).

[13] X.H. Li, Y. He, L. Jiao, *et al.*, "Vertical random vibration response and optimization of cutting head based on parameter identification", *China Mech. Eng.* 26 (6), 818–823 (2015).

[14] Q. Zhang, H.J. Wang, Z. Wang, *et al.*, "Analysis of coal-rock's cutting characteristics and flash temperature for peak based on infrared thermal image testing", *Chinese J. Sens. Actuators* 29 (5), 686–692 (2016).

[15] X.Y. Wang, Z.W. Jiang, Y.L. Yu, *et al.*, "Research on multi-information fusion technique for diagnosis of urban gas pipeline leakage", *China Saf. Sci. J.* 24 (6), 165–170 (2014).

[16] J.H. Hu, Z.H. Yu, X.S. Zhai, *et al.*, "Research of decision fusion diagnosis of aero-engine rotor fault based on improved D-S theory", *Acta Aeronaut. ETA Astronaut. Sinica.* 35 (2), 436–443 (2014).

[17] B. Wyrwołof, "Linguistic decomposition technique based on partitioning the knowledge base of the fuzzy inference system", *Bull. Pol. Ac.: Tech.* 56 (1), 71–76 (2008).

[18] A. Mreła, O. Sokolov, and W. Urbaniak, "The method of learning outcomes assessment based on fuzzy relations", *Bull. Pol. Ac.: Tech.* 67 (3), 527–533 (2019).

[19] H.J. Wang and Q. Zhang, "Dynamic identification of coal-rock interface based on adaptive weight optimization and multi-sensor information fusion", *Inf. Fusion.* 51 (11), 114–128 (2019).

[20] X. Zhang and L.H. Mou, "Research on compound protection for mine power network based on information fusion", *J. China Coal Soc.* 37 (11), 1947–1952 (2012).

[21] X.M. Liu, L.H. Mou, and X. Zhang, "Failure diagnosis for storage-capacitor in permanent magnetic actuator of flame proof switch gear based on information fusion", *J. China Coal Soc.* 39 (10), 2121–2127 (2014).

[22] A.F. Zhu, Z.R. Jing, W.J. Chen, *et al.*, "Data fusion based on ANFIS and evidence theory", *Journal of North University of China* (Natural Science Edition) 30 (1), 74–79 (2009).

[23] J.C. Zhang, S.P. Zhou, Y. Li, *et al.*, "Improved D-S evidence theory for pipeline damage identification", *J. Vibroeng.* 17 (7), 3527–3537 (2015).

[24] Y.L. Guo, Y. Liu, Q.Y. Du, *et al.*, "The identification research of emergency treatment technology for sudden heavy metal pollution accidents in drainage basin based on D-S evidence theory", *Water Sci. Technol.* 80 (12), 2392–2403 (2020).

[25] T. Chen, L. Chen, Y.F. Cai, *et al.*, "Estimation of vehicle sideslip angle via pseudo-multisensor information fusion method", *Bull. Pol. Ac.: Tech.* 25 (3), 499–516 (2018).